Testing, modelling and design of 7A04-T6 high-strength aluminium alloy RHS columns under axial compression

Li, Beibei; Wang, Yuanqing; Zhi, Xinhang; Zhang, Ying; Baniotopoulos, Charalampos C.

DOI:
10.1016/j.jobe.2022.104910

Document Version
Peer reviewed version

Citation for published version (Harvard):
Li, B, Wang, Y, Zhi, X, Zhang, Y & Baniotopoulos, CC 2022, 'Testing, modelling and design of 7A04-T6 high-strength aluminium alloy RHS columns under axial compression', *Journal of Building Engineering*, vol. 57, 104910. https://doi.org/10.1016/j.jobe.2022.104910

Testing, modelling and design of 7A04-T6 high-strength aluminium alloy RHS columns under axial compression

Beibei Li[a], Yuanqing Wang[a,b], Xinhang Zhi[a,*] (corresponding author), Ying Zhang[a], Charalampos C.Baniotopoulos[c]

[a] *Department of Civil Engineering, Tsinghua University, Beijing 100084, PR China*
[b] *Key Laboratory of Civil Engineering Safety and Durability of China Ministry of Education, Tsinghua University, Beijing 100084, PR China;*
[c] *School of Engineering, University of Birmingham, Edgbaston, Birmingham, B15 2TT, UK*

ABSTRACT: The buckling behaviour and resistances of extruded 7A04-T6 high-strength aluminium alloy rectangular hollow section (RHS) columns under axial compression are reported in this paper. Nineteen RHS columns with member relative slenderness of 0.44-2.70 and cross-sections of Class 2-4 were conducted. Finite element (FE) models were developed and verified against the test failure modes, axial load-end shortening or mid-height lateral displacement curves and buckling resistances, and parametric analyses with a wide range of member and cross-section slenderness were performed. The generated test and FE results of 7A04-T6 high-strength aluminium alloy RHS columns were compared with current design methods specified in Chinese, European, American and Australian/New Zealand codes. The results indicated that the former three standards yielded conservative flexural buckling resistance predictions by about 9%, while slightly unsafe results were found for Australian/New Zealand standard, with all satisfactory reliability level. However, Chinese code resulted in the most conservative local-flexural buckling resistance predictions by about 35%, while conservative results under smaller member slenderness and overestimated ones under larger member slenderness were observed for other three standards, leading to scattered data and failing to reach target reliability indices. A series of improved design approaches shown to be safe and efficient for 7A04-T6 high-strength aluminium alloy RHS columns were suggested and validated by reliability analyses, including modified design curves for RHS columns to flexural buckling on Chinese and American standards, and three ways of proposals to

imperfection terms with new coefficients as well as the direct strength method (DSM) in the framework of Chinese standard for RHS columns to local-flexural buckling.

KEYWORDS

High-strength aluminium alloy; Rectangular hollow section (RHS); Column test; Finite element (FE) analysis; Flexural and interactive buckling

1. Introduction

Aluminium alloys are being increasingly employed to spatial structures, bridges and towers, primarily owing to their good corrosion resistance, natural aesthetics, and flexible access to various cross-section shapes over structural steels [1]. Most of these structural members are made of extruded 5xxx and 6xxx series aluminium alloys with nominal yield strengths ($f_{0.2}$) less than 300 MPa, which are also specified in Chinese code (GB 50429-2007) [2], European standard (EN 1999-1-1:2007) [3], American specification (AA-2015) [4] and Australian/New Zealand standard (AS/NZS 1664.1:1997) [5]. However, with the development of modern structures toward long-span and high-rise structures under complex and heavy loading conditions, greater cross-section members are inevitably required to produce higher structural resistances using the codified normal-strength aluminium alloys, which may be in excess of the cross-section limits under the existing extrusion technology. For example, in design of the spatial reticulated shell (i.e. Usnisa Palace in Nanjing, China) with structural span up to about 200 m [6, 7], the extruded 6061-T6 aluminium alloy box-section members with maximum profiles of 550-mm height and 290-mm width were adopted after careful optimization. High-strength aluminium alloys, such as the 7A04-T6 and 7075-T6 with yield strengths up to about 500 MPa, are considered as promising high-performance construction materials, which can significantly reduce the cross-section dimensions of structural members, and thereby facilitates transportation and on-site assembly as well as avoiding inaccessible extrusion process of super-large cross-section members. The chemical compositions

between 7xxx series high-strength aluminium alloys (e.g., 7A04-T6) and 6xxx series normal-strength aluminium alloys (e.g., 6061-T6) are obviously different, resulting in significantly variants in material strength, ductility, toughness and ratio of yield to ultimate strength, which finally affects the structural behavior of aluminium alloy members. For example, the influence of initial geometric imperfections on the axial compression resistances of columns would decrease with the increase of material strength. Therefore, the structural performance of high-strength aluminium alloy columns should be independently studied relative to normal-strength aluminium alloy columns. However, the lack of codified design rules and limited experimental studies poses a limitation of applications of high-strength aluminium alloys in structural engineering.

To date, sufficient studies on normal-strength aluminium alloy columns subjected to axial compression are available in the literature, such as the 6061-T6 and 6063-T5 square, rectangular and circular hollow section (SHS/RHS/CHS) and channel section columns in Zhu and Young [8-10], Zhu et al. [11] and Su et al. [12], 6082-T6 H-section and RHS columns in Adeoti et al. [13], 6061-T6 and 6063-T5 H-section and RHS columns in Wang et al. [6, 14], 6061-T6 and 6063-T5 SHS and RHS columns with openings in Feng, Young and Liu [15, 16], and 5052-H32 built-up channel section columns in Roy et al. [17] and Fang et al. [18].

Nevertheless, limited investigations have been performed on the material properties, structural behaviour of 7xxx series high-strength aluminium alloy members. Specifically, Wang et al. [19] and Yun et al. [20] calibrated the cyclic and monotonic stress-strain constitutive relationships of the 7A04-T6 high-strength aluminium alloy. Wang et al. [21, 22] studied the axial compression buckling performance of fixed-ended and pin-ended 7A04-T6 high-strength aluminium alloy angle columns, with the results indicating that the relevant design approaches yielding good predicted resistances of angle columns undergoing flexural buckling, but highlighting the inapplicability for angle columns subjected to flexural-torsional buckling.

Rong et al. [23] carried out the axial compression tests on 7A04-T6 high-strength aluminium alloy SHS and RHS columns, and the results obtained from current codified design buckling curves were generally conservatism. The flexural buckling resistances of 7075-T6 high-strength aluminium alloy H-section columns subjected to axial compression were experimentally studied by Yuan et al. [24], where current design methods were assessed and a new buckling curve was suggested. Additionally, eccentric loading tests on 7A04-T6 high-strength aluminium alloy SHS, RHS and CHS columns were conducted by Hu et al. [25] and Rong et al. [26] to investigate the combined compression and bending behaviour, and the conservative prediction results of codified provisions were highlighted except for the overestimation in the case of CHS columns with larger member slenderness under smaller eccentricity ratio using EN 1999-1-1:2007. However, the flexural buckling and local-flexural buckling behavior of 7A04-T6 high-strength aluminium alloy RHS columns remains relatively scarce.

Therefore, an experimental programme into extruded 7A04-T6 high-strength aluminium alloy RHS columns was firstly performed. A finite element (FE) modelling analysis was then carried out, where FE models were established and verified against corresponding test results, and parametric studies with a wide range of member and cross-section slenderness were conducted. The axial compression resistances obtained from the test and FE results were subsequently used to assess the applicability of current codified design rules for 7A04-T6 high-strength aluminium alloy RHS columns to flexural buckling and local-flexural buckling, as set out in GB 50429-2007, EN 1999-1-1:2007, AA-2015 and AS/NZS 1664.1:1997. Finally, a series of improved design approaches were suggested and validated by reliability analyses.

2. Experimental studies

2.1 Test specimens

In order to investigate the flexural buckling and local-flexural interactive buckling behaviour of extruded

7A04-T6 high-strength aluminium alloy RHS columns, three cross-sections, including Class 2 and 3 for flexural buckling and Class 4 for both flexural buckling and local-flexural interactive buckling, were designed. The classification of cross-sections was determined according to EN 1999-1-1:2007 [3]. Additionally, various member lengths with low, medium and high member relative slenderness were considered for each cross-section to cover potential member lengths in engineering practice. The criteria for selecting the lengths of specimens failed by local-flexural buckling is that the cross-section elastic local buckling stress (σ_{cr}) is less than its member flexural buckling stress (σ_{fb}). A total of nineteen specimens were tested under axial compression, and the measured dimensions of specimens are listed in Table 1, with symbols shown in Fig. 1, where A_g is the gross cross-section area, L denotes the column geometric length, L_e represents the distance from top to bottom knife edges ($L_e = L$+124 mm), and $\bar{\lambda}_g$ is the member relative slenderness about the minor axis, which is given by $\bar{\lambda}_g = [(f_{0.2}A_g)/N_{cr}]^{0.5}$, hereinto $f_{0.2}$ is the 0.2% proof (or nominal yield) stress, and N_{cr} signifies the Euler buckling load on the basis of A_g. All specimens were labelled by the section type, loading configuration, cross-section dimensions and slenderness. Take RAC100-70-8-16 as an example, it indicates a rectangular column subjected to axial compression with a nominal cross-section width of 100 mm, height of 70 mm and thickness of 8 mm, and the member slenderness ($\lambda = L_e/i_c$) is 16, in which i_c is the cross-section radius of gyration about the minor axis.

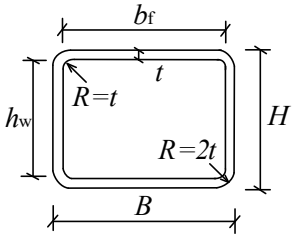

Fig. 1. Schematic diagram of the cross-section

Table 1. Measured dimensions of specimens

Specimen	B (mm)	H (mm)	t (mm)	A_g(mm^2)	L (mm)	L_e (mm)	$\bar{\lambda}_g$
RAC100-70-8-16	100.54	70.12	8.52	1527.7	299.8	423.8	0.44
RAC100-70-8-32	100.53	70.18	8.61	1522.7	699.5	823.5	0.85
RAC100-70-8-47	100.52	70.26	8.53	1526.3	1099.0	1223.0	1.26

RAC100-70-8-62	100.8	70.2	8.47	1516.8	1503.2	1627.2	1.68
RAC100-70-8-77	100.36	70.44	8.48	1532.5	1899.1	2023.1	2.08
RAC100-70-8-93	100.51	70.29	8.52	1546.6	2299.0	2423.0	2.50
RAC100-50-6-17	99.84	49.21	5.89	2430.7	201.2	325.2	0.47
RAC100-50-6-33	99.8	49.2	5.87	2452.2	500.8	624.8	0.91
RAC100-50-6-48	99.74	49.19	5.89	2435.1	800.0	924.0	1.34
RAC100-50-6-62	99.77	49.1	5.85	2425.0	1050.8	1174.8	1.71
RAC100-50-6-77	99.73	49.35	5.91	2423.9	1350.5	1474.5	2.13
RAC100-50-6-92	99.86	49.48	5.96	2433.1	1647.3	1771.3	2.56
RAC60-30-3-31	60.2	30.26	3.06	492.0	249.8	373.8	0.83
RAC60-30-3-45	60.13	30.29	3.07	493.2	429.1	541.1	1.20
RAC60-30-3-61	60.22	30.13	3.03	487.2	600.2	724.2	1.61
RAC60-30-3-72	60.28	30.15	3.04	489.0	740.4	864.4	1.92
RAC60-30-3-76	60.44	30.23	3.06	493.3	800.4	912.4	2.03
RAC60-30-3-92	60.2	30.24	3.10	497.5	970.8	1094.8	2.44
RAC60-30-3-101	60.35	30.23	3.10	498.4	1100.5	1212.50	2.70

2.2 Material properties

According to GB/T 228.1-2010 [27], three repeated coupons along the extruded direction were respectively extracted from the middle part of three walls of each cross-section, as shown in Fig. 2 (a), and they were then monotonically loaded in a hydraulic testing machine with capacity of 1000 kN. The measured stress-strain curves of the 7A04-T6 high-strength aluminium alloy are illustrated in Fig. 2, while the key average measured parameters of Young's modulus (E), nominal yield stress ($f_{0.2}$), ultimate stress (f_u), ultimate strain at f_u (ε_u) and exponent of the Ramberg-Osgood (R-O) expression (n) are tabulated in Table 2. Note that the exponent parameter (n) was computed by $n = \ln(0.002/\varepsilon_{0,u})/\ln(f_{0.2}/f_u)$ [20], in which $\varepsilon_{o,u}=\varepsilon_u-0.002$.

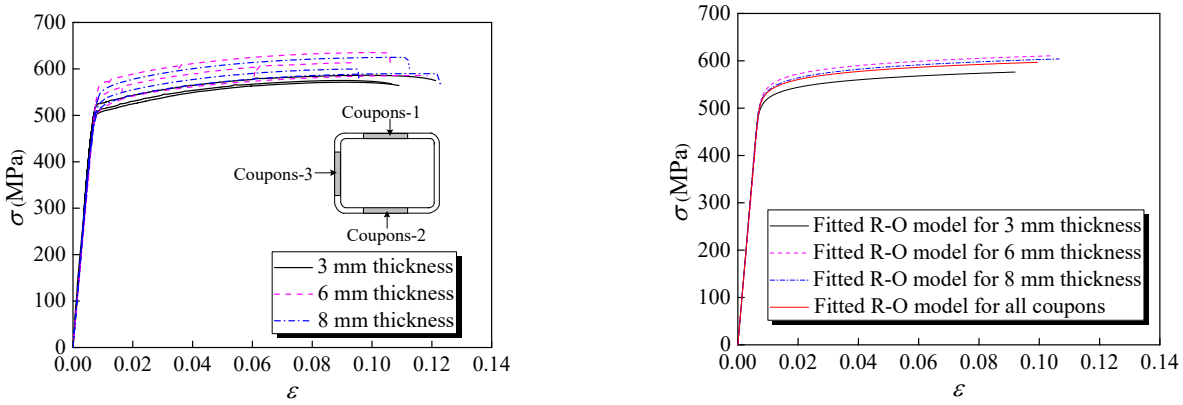

(a) Measured stress-strain curves (b) Predicted stress-strain curves

Fig. 2. Measured and predicted stress-strain curves

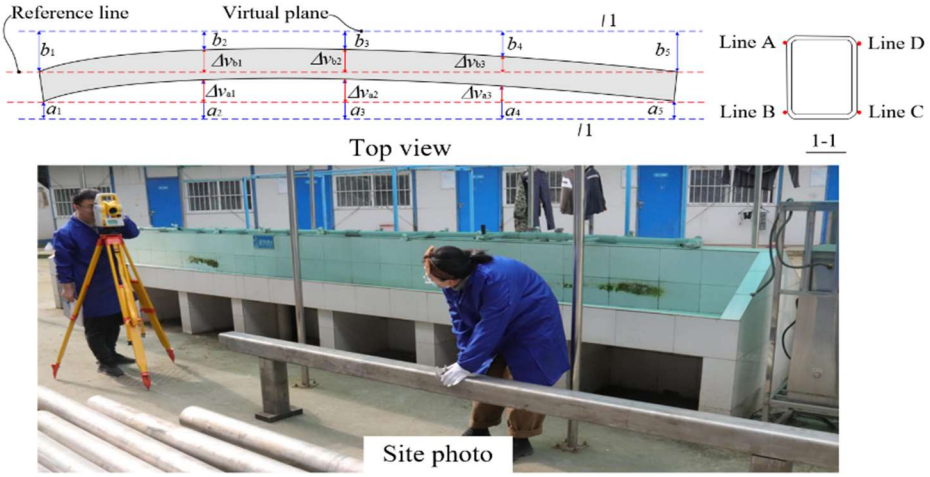

Fig. 3. Schematic diagram of initial geometrical imperfection measurements

Table 2. Measured material properties

Section ($B\times H\times t$)	Thickness (mm)	E (GPa)	$f_{0.1}$ (MPa)	$f_{0.2}$ (MPa)	f_u (MPa)	ε_u (%)	n
60×30×3 mm	3	73.64	510.37	514.49	577.53	9.22	32.99
100×50×6 mm	6	71.27	534.83	540.93	611.57	10.16	31.93
100×70×8 mm	8	74.70	512.37	530.83	604.72	10.47	30.18
Mean	-	73.20	519.19	528.75	597.94	9.95	31.70
COV	-	0.021	0.040	0.038	0.035	0.097	0.067

2.3 Initial global geometric imperfections and loading eccentricities

The initial global geometric imperfections about the minor axis of specimens were measured using a total station and a vernier caliper [28], as displayed in Fig. 3. Deviations (e.g. a_1, a_2, a_3, a_4 and a_5) between the measuring points along both ends, mid-height and quarter length of the column longitudinal edge line (i.e. line A, B, C and D) and virtual plane formed by the total station were first measured. Then, the out-of-straightness of each longitudinal edge line relative to the reference line defined by the column ends (e.g. Δv_{a1}, Δv_{a2} and Δv_{a3}) can be computed according to the geometric relationship. The maximum values among Δv_1, Δv_2 and Δv_3 (e.g. $\Delta v_1 = (\Delta v_{a1}+\Delta v_{b1}+\Delta v_{c1}+\Delta v_{d1})/4$) were taken as the initial global geometric imperfections (w_g), as shown in Table 3. Besides, the loading eccentricities about the minor axis at the top and bottom ends of columns (e_{ct} and e_{cb}) were calculated with the combination of strain gauges at column ends and applied load using $e_c = M/N = (W_{el}\varepsilon_M)/(A_g\varepsilon_N)$, in which W_{el} is the elastic cross-section

modulus, ε_M and ε_N are the strains caused by pure bending and axial compression, respectively. Note that the strains corresponding to $0.15N_u$ at column ends were adopted to compute loading eccentricities to ensure that all specimens were elastically and stably compressed [29], in which N_u is the axial compression resistance of specimens. The equivalent initial imperfections are given by $e_{eq} = e_c + w_g$ and listed in Table 3. It showed that the initial global geometric imperfections were significantly below $L/1000$, while the equivalent initial imperfections were within the range of $(0.5\text{-}3.63)L/1000$.

Table 3. Measured global geometric imperfections and loading eccentricities of specimens

Specimen	w_g (mm)	e_{ct} (mm)	e_{cb} (mm)	e_{eq} (mm)	w_g/L (‰)	e_{eq}/L (‰)
RAC100-70-8-16	0.10	0.13	1.07	0.70	0.33	2.33
RAC100-70-8-32	0.23	1.61	1.11	1.59	0.33	2.27
RAC100-70-8-47	0.35	0.34	0.63	0.84	0.32	0.76
RAC100-70-8-62	0.54	1.28	-0.85	0.76	0.36	0.50
RAC100-70-8-77	0.64	0.13	0.54	0.98	0.34	0.51
RAC100-70-8-93	1.86	1.49	1.53	3.37	0.81	1.47
RAC100-50-6-17	0.10	1.38	1.38	1.48	0.50	7.36
RAC100-50-6-33	0.15	1.56	1.33	1.60	0.30	3.18
RAC100-50-6-48	0.37	-0.91	1.27	0.55	0.46	0.69
RAC100-50-6-62	0.41	0.44	0.8	1.03	0.39	0.98
RAC100-50-6-77	0.91	1.4	2.21	2.72	0.67	2.01
RAC100-50-6-92	1.07	1.34	1.26	2.37	0.65	1.44
RAC60-30-3-31	0.23	-0.27	0.87	0.53	0.92	2.12
RAC60-30-3-45	0.27	0.34	0.34	0.61	0.63	1.42
RAC60-30-3-61	0.31	1.04	2.7	2.18	0.52	3.63
RAC60-30-3-72	0.41	0.28	1.95	1.53	0.55	2.06
RAC60-30-3-76	0.62	0.41	0.25	0.95	0.77	1.19
RAC60-30-3-92	0.49	0.16	1.06	1.10	0.50	1.13
RAC60-30-3-101	1.17	4.44	0.24	3.51	1.06	3.19

2.4 Test setup and instrument configurations

All specimens were concentrically loaded in a servo-control hydraulic compression machine with capacity of 5000 kN, as shown in Figs. 4 and 5. The constant rate of 0.4 mm/min was adopted during displacement-control loading process. The load, displacement and strain responses were recorded using the DH3816N Static Strain Acquisition System.

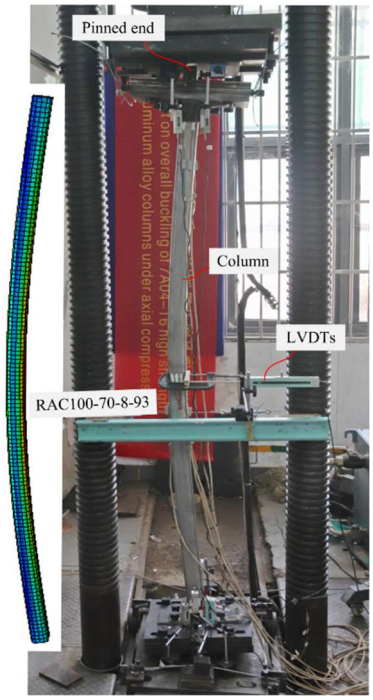

Fig. 4. Test setup and flexural buckling of specimen RAC100-70-8-93

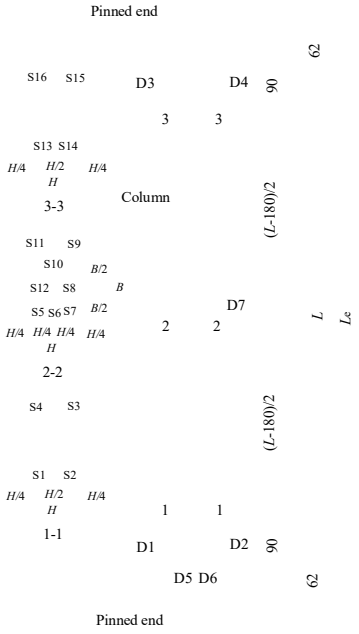

Fig. 5. Layout of LVDTs and strain gauges

The knife hinge configurations, releasing free rotations about the minor axis, were arranged to achieve pin-ended boundary conditions for specimens. Meanwhile, the angle clamping devices were tightly bolted at the top and bottom ends to fix specimen ends during loading process. Note that the effective member length (L_e) of all specimens listed in Table 1 equal to $L_e = L + 124$ mm, as shown in Fig. 5. Four linear LVDTs (i.e. D1, D2, D3 and D4) were arranged at the top and bottom end bearing supports to monitor their rotations, as illustrated in Fig. 5. Two LVDTs (i.e. D5 and D6) and one LVDT (i.e. D7) were respectively placed at the center of end bearing supports and mid-height of specimens to measure the end shortening and in-plane displacement. Additionally, a total of 16 strain gauges were attached at the mid-height section and the sections at a distance of 90 mm to the specimen ends to monitor the strain responses and quantify the loading eccentricities.

2.5 Test results

The overall flexural buckling mode occurred for all specimens, except for the specimen RAC60-30-3-31 with the low member slenderness and Class 4 cross-section who failed in the local-flexural buckling mode. The typical flexural buckling and local-flexural buckling modes are illustrated in Figs. 4 and 6,

respectively. Three groups of deformed columns after tests are presented in Fig. 7, and their failure modes were summarized in Table 4.

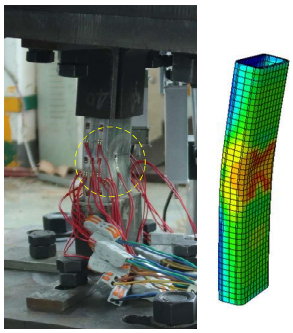

Fig. 6. Local-flexural buckling of specimen RAC60-30-31

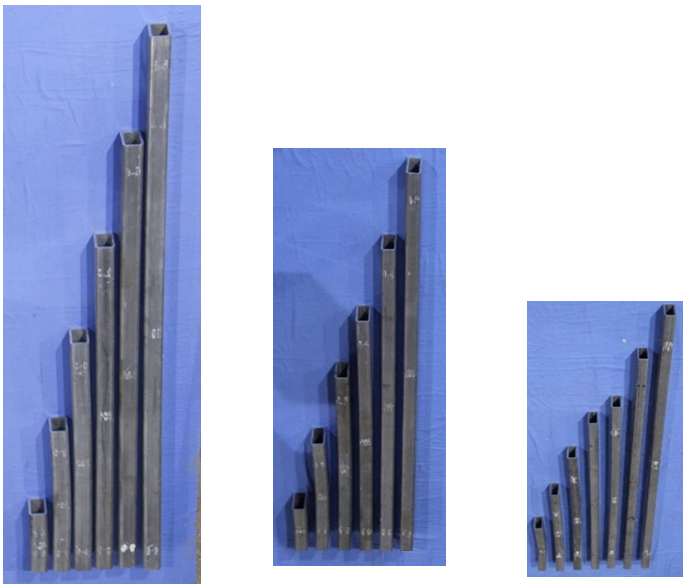

(a) RAC100-70-8 (b) RAC100-50-6 (c) RAC60-30-3

Fig. 7. Deformed specimens after testing

Table 4. Summarized experimental and numerical results of specimens

Specimen	Failure modes	$N_{u,exp}$ (kN)	$N_{u,FE}$ (kN)	$N_{u,FE}$ /$N_{u,exp}$
RAC100-70-8-16	F	1252.94	1250.75	1.00
RAC100-70-8-32	F	1070.74	1008.66	0.94
RAC100-70-8-47	F	761.30	720.53	0.95
RAC100-70-8-62	F	455.05	428.61	0.94
RAC100-70-8-77	F	290.80	280.23	0.96
RAC100-70-8-93	F	181.88	188.77	1.04
RAC100-50-6-17	F	711.21	741.47	1.04
RAC100-50-6-33	F	630.60	603.19	0.96
RAC100-50-6-48	F	432.23	421.29	0.97
RAC100-50-6-62	F	271.00	260.38	0.96
RAC100-50-6-77	F	156.70	164.21	1.05
RAC100-50-6-92	F	112.89	117.51	1.04
RAC60-30-3-31	F+L	250	211.15	1.04
RAC60-30-3-45	F	154.90	151.72	0.98
RAC60-30-3-61	F	83.98	81.26	0.97
RAC60-30-3-72	F	60.90	60.52	0.99
RAC60-30-3-76	F	59.84	57.87	0.97
RAC60-30-3-92	F	44.09	40.19	0.91
RAC60-30-3-101	F	33.00	31.94	0.97
Mean				0.98
COV				0.04

Note: The symbol “F” represents flexural buckling and “L” denotes local buckling.

The axial compression resistances of all specimens ($N_{u,exp}$) are reported in Table 4. The axial load versus end shortening curves for all specimens, and axial load versus mid-height lateral displacement curves for all except specimens RAC100-70-8-16 and RAC100-50-6-17, whose length were too short to arrange LVDTs at mid-height of columns, are illustrated in Fig. 8. It was found that the axial stiffness decreased with the increase of member relative slenderness. The axial load dropped significantly for specimens with small member relative slenderness after reaching their axial compression resistances, while this phenomenon became less obvious with the increase of member relative slenderness.

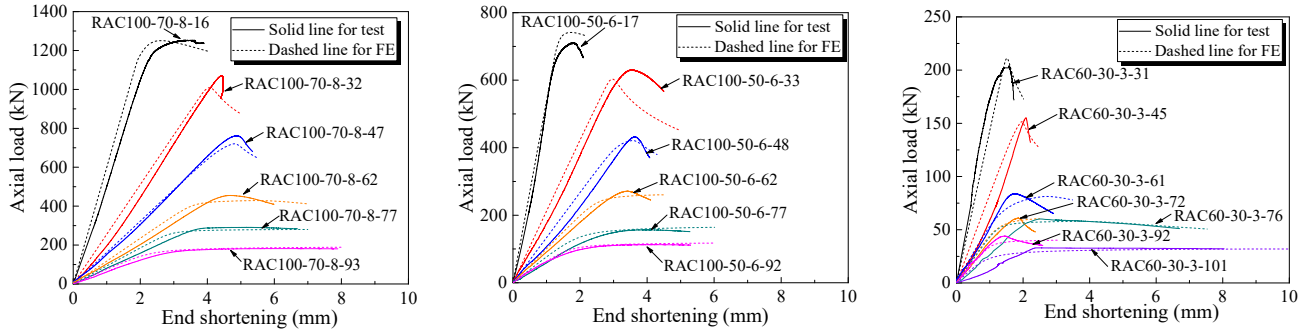

(a) Axial load-end shortening curves of specimens

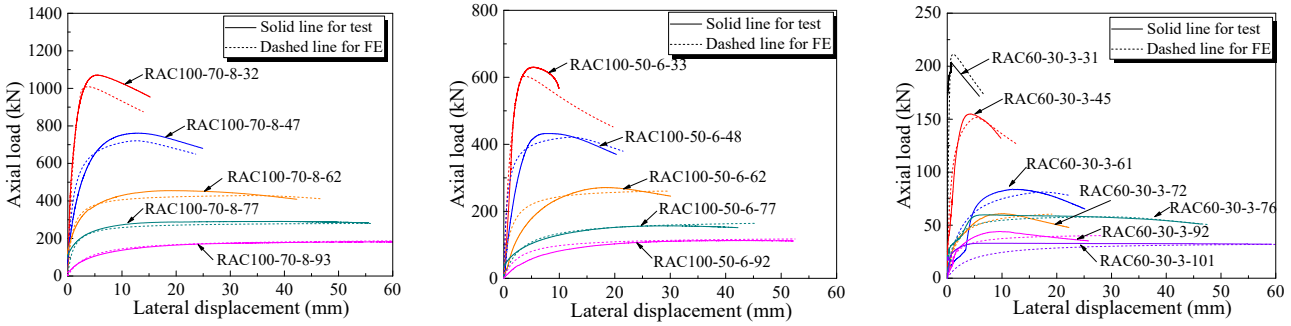

(b) Axial load-mid-height lateral displacement curves of specimens

Fig. 8. Axial load versus end shortening or lateral displacement curves of specimens

3. FE modelling and parametric studies

This section was to simulate the experimental results of 7A04-T6 high-strength aluminium alloy RHS columns to flexural buckling and local-flexural buckling under axial compression through FE analyses, and then establish a data pool to assess and further modify the current codified aluminium alloy design methods.

3.1 Finite element modelling

The incompatible-mode 8-node linear brick element C3D8I available in ABAQUS library [30],

exhibiting a good convergence and computational accuracy, was adopted in the FE models of test specimens. The true stress-logarithmic plastic strain curves originated from the average measured stress-strain curves shown in Fig. 2 were inputted into ABAQUS. Two reference points at top and bottom edge of knife hinge were created and coupled with the column end section. The pin-ended conditions were achieved by fixing all degrees of freedom of the two reference points, except for the rotation about the minor axis and the longitudinal translation of the top reference point. Note that the loading eccentricities were incorporated in FE models by offsetting two reference points with measured values listed in Table 3. According to the mesh sensitivity analyses, a mesh size of $2t \times 2t$ mm, with two elements across the thickness, was adopted because of a good balance between the sufficient computational accuracy and acceptable computational time.

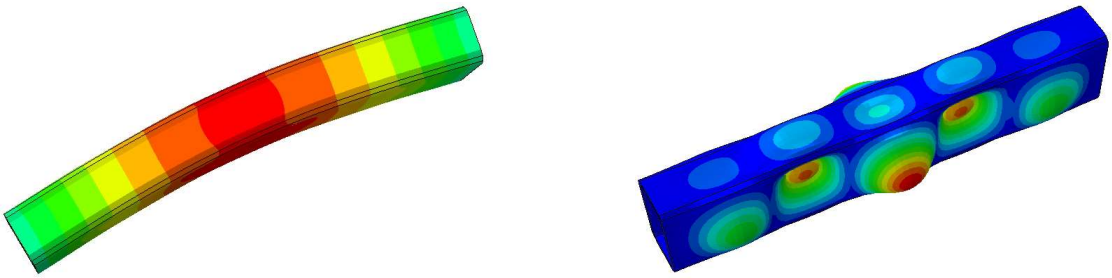

(a) Global buckling mode (b) Local buckling mode

Fig. 9. Global and local buckling shapes of FE models

The lowest global and local buckling modes were obtained by an eigenvalue buckling analysis shown in Fig. 9, which were then utilised to represent the initial global and local geometric imperfection types. The measured initial global geometric imperfections were introduced in FE models for specimens with Class 2 and 3 cross-sections, while both the local and global geometric imperfections were incorporated in FE models for specimens with Class 4 cross-section. Since the local geometric imperfection amplitudes were not measured, a total of 71 previously measured ones, which were conducted by Zhu et al. [8], Wang et al. [14], Yuan et al. [31] and Zhi et al. [32] for 6061-T6, 6063-T5 and 7075-T6 aluminium alloy columns, were collected and analyzed, as shown in Fig. 10. The formula given in Eq. (1) showed that the best fit was achieved in the form of $w_o/t=w_p(f_{0.2}/\sigma_{cr}')$ [33] with a corresponding coefficient of

determination R^2 of 0.37, in which $\sigma'_{cr} = 4\pi^2 E/[12(1-\nu^2)(b/t)^2]$, ν is the Poisson's ratio, b/t is the greatest width-to-thickness ratio of elements and expressed as b_f/t or h_w/t for RHS columns, w_p is the constant. The global imperfection amplitudes exhibited in Table 3 and the local ones derived from Eq. (1) were finally inputted into ABAQUS.

$$w_o/t=0.033(f_{0.2}/\sigma'_{cr}) \quad (1)$$

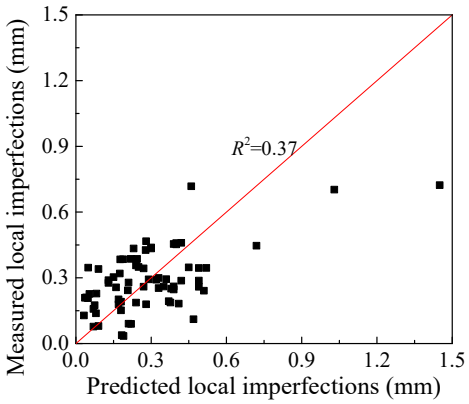

Fig. 10. Measured versus predicted local geometric imperfections

3.2 Validation of FE models

The simulated results of the failure modes, load versus end shortening or lateral displacement curves, and the buckling resistances were compared to experimental counterparts to evaluate the accuracy of the numerical modelling methodology. Figs. 4 and 6 indicate that the FE models successfully simulated the flexural buckling and local-flexural buckling modes observed in test specimens. The numerical load versus end shortening or lateral displacement curves were generally consistent with those of experimental results, as displayed in Fig. 8. The mean ratio of numerical-to-test buckling resistances of all specimens, shown in Table 4, was 0.98 with a coefficient of variation (COV) of 0.04, conforming the accuracy of the developed FE models. Overall, the FE models can provide accurate axial compression resistance predictions and can be applied to carry out parametric analyses.

3.3 Parametric studies

On the basis of verified FE models, extensive parametric studies were conducted to develop a more comprehensive investigation into the axial compression buckling behaviour of 7A04-T6 high-strength

aluminium alloy RHS columns. In total, 900 columns failing by flexural buckling, half of which buckling about the minor and major axes, respectively, were generated. The width-to-height ratio (B/H) and the width-to-thickness ratio of elements (b_f/t) were respectively within the range of 1.25-2.5 and 6-15 by changing cross-section width or height but keeping the thickness constant of 8 mm, covering Class 1-3 cross-sections, as tabulated in Table 5. Fifteen column lengths were designed for each cross-section with a wide range of $\bar{\lambda}_g$ from 0.3 to 3.0. Besides, parametric studies were also performed on 396 columns to local-flexural buckling about the minor axis, with B/H and b_f/t of 1.25-2.5 and 18-70, respectively, and the cross-sections were categorized as Class 4 with a constant thickness of 6 mm, as shown in Table 6. Various column lengths were specially selected to ensure the occurrence of local-flexural buckling mode under axial compression, based on the criterion that the cross-section elastic local buckling stress (σ_{cr}) is less than its member flexural buckling stress (σ_{fb}), with a wide range of $\bar{\lambda}_g$ between 0.3 and 3.0. Note that σ_{cr} and σ_{fb} are determined using the finite strip software CUFSM [34].

Table 5. Dimensions of columns to flexural buckling in the parametric studies (t = 8, unit: mm)

B/H b_f/t	1.25 $B\times H$	1.5 $B\times H$	1.75 $B\times H$	2.0 $B\times H$	2.5 $B\times H$
6	64×51	64×43	64×37	64×32	64×26
7	72×58	72×48	72×41	72×36	72×29
9	88×70	88×59	88×50	88×44	88×35
11	104×83	104×69	104×59	104×52	104×42
13	120×96	120×80	120×69	120×60	120×48
15	136×109	136×91	136×78	136×68	136×54

Table 6. Dimensions of columns to local-flexural buckling in the parametric studies (t = 6, unit: mm)

B/H b_f/t	1.25 $B\times H$	1.5 $B\times H$	1.75 $B\times H$	2.0 $B\times H$	2.5 $B\times H$	B/H b_f/t	1.25 $B\times H$	1.5 $B\times H$	1.75 $B\times H$	2.0 $B\times H$	2.5 $B\times H$
18	120×96	120×80	120×69	120×60	120×48	45	282×226	282×188	282×161	282×141	282×113
21	138×110	138×92	138×79	138×69	138×55	50	312×250	312×208	312×178	312×156	312×125
24	156×125	156×104	156×89	156×78	156×62	55	342×274	342×228	342×195	342×171	342×137
27	174×139	174×116	174×99	174×87	174×70	60	372×298	372×248	372×213	372×186	372×149
30	192×154	192×128	192×110	192×96	192×77	65	402×322	402×268	402×230	402×201	402×161
35	222×178	222×148	222×127	222×111	222×89	70	432×346	432×288	432×247	432×216	432×173
40	252,202	252,168	252×144	252×126	252×101						

The average measured material properties of E = 73.2 GPa, $f_{0.2}$ = 529 MPa, f_u = 598 MPa, ε_u = 9.95%

and n = 31.7 were employed in all FE models, as shown in Fig. 2 (b). Note that the out-of-plane deformation was restrained at the middle and quarter height of RHS columns for buckling about the major axis. Initial global geometric imperfection amplitudes of L/1000 were introduced in FE modes failing by flexural buckling, while combinations of initial local geometric imperfections from Eq. (1) and global geometric imperfections of L/1000 were considered in FE models to local-flexural buckling. The axial compression resistances from the test and FE analyses were utilized to evaluate the accuracy and reliability of current codified and relevant modified design methods for 7A04-T6 high-strength aluminium alloy RHS columns in the following sections.

4. Comparisons with current codified and modified design methods

4.1 Chinese standard (GB 50429-2007)

The Perry-Roberson buckling formulae characterized with imperfection parameters are adopted in GB 50429-2007 [2] to compute the axial compression buckling resistances of extruded aluminium alloy RHS columns, as given by Eq. (2)

$$N_{u,GB} = \chi_{GB} f_{0.2} A_{e,GB} / \gamma_{R,GB} \quad (2)$$

where $\gamma_{R,GB}$ is the partial safety factor of 1.2; $A_{e,GB}$ is the gross cross-section area (A_g) when $b/t \leq 21.5(240/f_{0.2})^{0.5}$, while the effective cross-section area shall be used when $b/t > 21.5(240/f_{0.2})^{0.5}$, and $A_{e,GB}$ can be calculated according to the effective thickness method using the Winter-form equation $t_e = (1/\bar{\lambda} - 0.22/\bar{\lambda})t$ and $\bar{\lambda} = (f_{0.2}/\sigma'_{cr})^{0.5}$; χ_{GB} is the buckling reduction factor and expressed by $\chi_{GB} = (\phi + \sqrt{\phi^2 - \bar{\lambda}_g^2})^{-1}$, hereinto $\phi = 0.5(1 + \eta + \bar{\lambda}_g^2)$, $\eta = \alpha(\bar{\lambda}_g - \bar{\lambda}_0)$, α and $\bar{\lambda}_0$ are the constants related to imperfection factor and limiting slenderness and set as 0.2 and 0.15, respectively.

4.2 European standard (EN 1999-1-1:2007)

The design provisions in EN 1999-1-1:2007 [3] for the calculation of axial compression buckling resistances of extruded aluminium alloy RHS columns are similar to those in GB 50429-2007, as given

by Eq. (3)

$$N_{u,EN} = \chi_{EN} f_{0.2} A_{e,EN} / \gamma_{R,EN} \quad (3)$$

where $\gamma_{R,EN}$ is the partial safety factor taken as 1.1; $A_{e,EN}$ is the gross cross-section area (A_g) for Class 1, 2 and 3 cross-sections and the relevant formulae are the same as those of GB 50429-2007, except for α and $\bar{\lambda}_0$ being 0.2 and 0.1, respectively. Different from GB 50429-2007, EN 1999-1-1:2007 takes the effective cross-section area ($A_{e,EN}$) into consideration when determining the buckling reduction factor (χ_{EN}), and that is $\chi_{EN} = (\phi + \sqrt{\phi^2 - \bar{\lambda}_{e,EN}^2})^{-1}$, $\phi = 0.5(1 + \eta + \bar{\lambda}_{e,EN}^2)$, $\eta = 0.2(\bar{\lambda}_{e,EN} - 0.1)$ and $\bar{\lambda}_{e,EN} = \sqrt{(f_{0.2} A_{e,EN}) / N_{cr}}$.

4.3 American design manual (AA-2015)

With regard to AA-2015 [4], the axial compression resistances of extruded aluminium alloy RHS columns are the least strength among three failure modes, i.e. the flexural buckling, local buckling and local-flexural buckling, which can be calculated from Eq. (4)

$$N_{u,AA} = \min(\phi_c f_c A_g,\ \phi_c \left[\sum_{i=1}^{n} f_{ci} A_i + f_{0.2}(A_g - \sum_{i=1}^{n} A_i)\right],\ \phi_c (0.85\pi^2 E/\lambda^2)^{1/3} f_e^{2/3} A_g) \quad (4)$$

where ϕ_c is the partial safety factor and equal to 0.9; f_c represents the compressive critical stress and can be determined from Eq. (5)

$$f_c = \begin{cases} f_{0.2} & \text{for } \lambda \le \lambda_1 \\ (B_c - D_c \lambda)[0.85 + 0.15(C_c - \lambda)/(C_c - \lambda_1)] & \text{for } \lambda_1 < \lambda \le C_c \\ 0.85\pi^2 E / \lambda^2 & \text{for } \lambda \ge C_c \end{cases} \quad (5)$$

where $\lambda_1 = (B_c - f_{0.2})/D_c$; B_c, C_c and D_c are the buckling constants and can be referred to Table B.4.2 in AA-2015; f_{ci} denotes the local buckling stress of element i determined using Section B.5.4.2 of AA-2015; A_i is the area of element i; f_e signifies the smallest elastic local buckling stress of all elements for a section and expressed as $\pi^2 E/(1.6b/t)^2$. Additionally, AA-2015 offers an alternative to obtain the local buckling strength and the local-flexural buckling strength determined by the direct strength method (DSM), and f_{ci} is obtained using Section B.5.4.6 of AA-2015; f_e is the elastic local buckling stress of a section, which

is equivalent to σ_{cr} described in Section 3.3.

4.4 Australian/New Zealand Standard (AS/NZS 1664.1:1997)

AS/NZS 1664.1:1997 [5] uses a similar design approach for the computation of the buckling resistances of axial compression loaded extruded aluminium alloy RHS columns as that specified in AA-2015, which can be calculated using Eq. (6)

$$N_{u,AS/NZS} = \min(\phi_{cc} f_{cc} A_g,\ \phi_{cc}\left[\sum_{i=1}^{n} f_{ci} A_i + f_{0.2}(A_g - \sum_{i=1}^{n} A_i)\right],\ \phi_u(\pi^2 E/\lambda^2)^{1/3} f_e^{2/3} A_g) \quad (6)$$

Three differences should be noted between the two standards: (1) a coefficient k_c = 1.12 is taken into account for columns within the slenderness plateau; (2) the partial safety factor ϕ_{cc} is related to the member relative slenderness but less than 0.95, and that is ϕ_{cc} = 1-0.21$\bar{\lambda}_g$ for $\bar{\lambda}_g \leq 1.2$ and ϕ_{cc} = 0.14$\bar{\lambda}_g$+0.58 for $\bar{\lambda}_g > 1.2$. Additionally, the partial safety factor ϕ_u is for the ultimate state of local-flexural buckling equaling to 0.85; and (3) the initial imperfections associated with bending and loading eccentricities are not taken into account.

4.5 Assessment of the codified and relevant modified design methods

The test and FE results of 7A04-T6 high-strength aluminium alloy RHS columns subjected to flexural buckling or local-flexural buckling were evaluated against the current column design methods. Note that the aforementioned partial safety factors should be set to unity to calculate their nominal strengths. The test results from the work of Rong et al. [23] on axial compression loaded RHS columns were also taken into account in the following analyses.

4.5.1 Columns to flexural buckling

The comparisons between test/FE results and column flexural buckling curves specified in the four standards are illustrated in Figs. 11 and 12. The mean ratios of test/FE-to-predicted resistances with their COVs are listed in Table 7. Overall, the predicted resistances of GB 50429-2007, EN 1999-1-1:2007 and AA-2015 for columns to member overall buckling were generally conservative by about 9%, with

corresponding COVs of 0.035, 0.036 and 0.048, indicating GB 50429-2007 design curve offered least scattered results. The AS/NZS 1664.1:1997 predictions were slightly unsafe and the most scattered among the four standards, with the mean ratio of $N_{u,exp/FE}/N_{u,AS/NZS}$ and COV being 0.987 and 0.062, respectively. This is primarily attributed to the ignorance of initial imperfections.

In order to achieve a higher level of accuracy for calculating the flexural buckling resistances of extruded 7A04-T6 high-strength aluminium alloy RHS columns, modifications to GB 50429-2007 and AA-2015 were performed. A new set of coefficients related to α and $\bar{\lambda}_0$ were proposed to be 0.16 and 0.28, respectively, for GB 50429-2007, meanwhile, the effective cross-section area ($A_{e,GB}$) shall be employed to calculate the flexural buckling reduction factor (χ_{GB}). The constants of 0.85 and 0.15 in Eq. (5) were modified to be 0.9 and 0.1, respectively, for AA-2015. The modified buckling curves for GB 50429-2007 and AA-2015 were closer to the test/FE data, as shown in Figs. 11 and 12, with the mean ratios of $N_{u,exp/FE}/N_{u,GB,MF}$ and $N_{u,exp/FE}/N_{u,AA,MF}$ being 1.045 and 1.041, and corresponding COVs being 0.024 and 0.032, lying marginally on the safe side with reduced scatters.

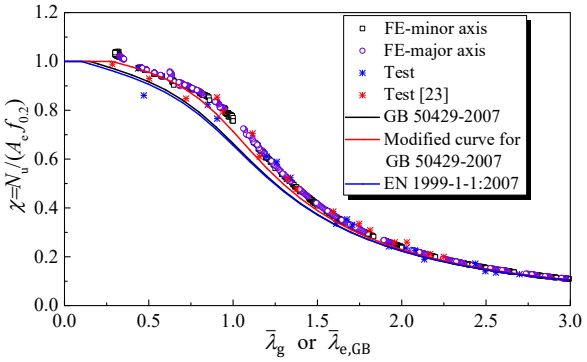

Fig. 11. Comparison of test/FE data with GB 50429-2007, modified GB 50429-2007 and EN 1999-1-1:2007 for columns to flexural buckling

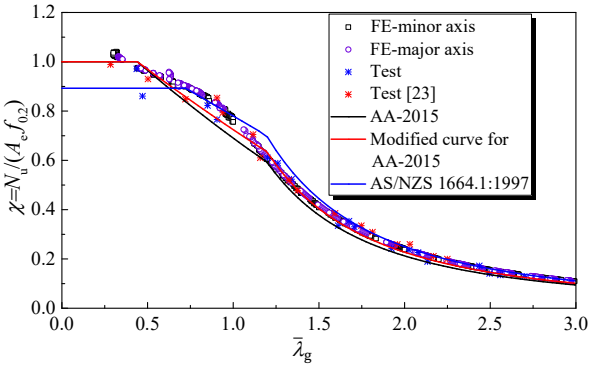

Fig. 12. Comparison of test/FE data with AA-2015, modified AA-2015 and AS/NZS 1664.1:1997 for columns to flexural buckling

Table 7. Comparison of test/FE results with predicted strengths for columns to flexural buckling

Ratio	$N_{u,exp/FE}$ /$N_{u,GB}$	$N_{u,exp/FE}$ /$N_{u,EN}$	$N_{u,exp/FE}$ /$N_{u,AA}$	$N_{u,exp/FE}$ /$N_{u,AS/NZS}$	$N_{u,exp/FE}$ /$N_{u,GB,MF}$	$N_{u,exp/FE}$ /$N_{u,AA,MF}$
Mean	1.086	1.093	1.096	0.987	1.045	1.041
COV	0.035	0.036	0.048	0.062	0.024	0.032

4.5.2 Columns to local-flexural buckling

The local-flexural buckling curves from GB 50429-2007 and EN 1999-1-1:2007 were plotted against the test and numerical axial compression resistances of 7A04-T6 high-strength aluminium alloy RHS columns, as illustrated in Figs. 13 and 14. There is no design buckling curves of AA-2015 and AS/NZS 1664.1:1997 in the form of member relative slenderness against buckling reduction factor because their load-carrying capacities were the least one among three failure modes.

It was found that the buckling curve from GB 50429-2007 was significantly below the experimental and numerical data points, revealing the most conservative predictions by approximately 35%, with the very high COV of 0.170. This may be due to the employment of A_g for determining χ_{GB} rather than $A_{e,GB}$. Conservative results under smaller member relative slenderness but overestimated ones under larger member relative slenderness were observed for EN 1999-1-1:2007. Meanwhile, similar predicted results were also found for AA-2015 and AS/NZS 1664.1:1997. Table 8 lists the predicted resistances for local-flexural buckling, in which $N_{u,AA}$ and $N_{u,AA\text{-}DSM}$ are the calculated resistances according to general provisions and alternative DSM in AA-2015. The predicted resistances obtained from EN 1999-1-1:2007, AA-2015 and AS/NZS 1664.1:1997 were all slightly greater than those of test and numerical results, with more scattered COVs of around 0.120 than those of columns to flexural buckling. It can be concluded that all the current standards fail to predict the axial compression resistances of RHS columns to local-flexural buckling, highlighting the need for the development of more accurate design approaches.

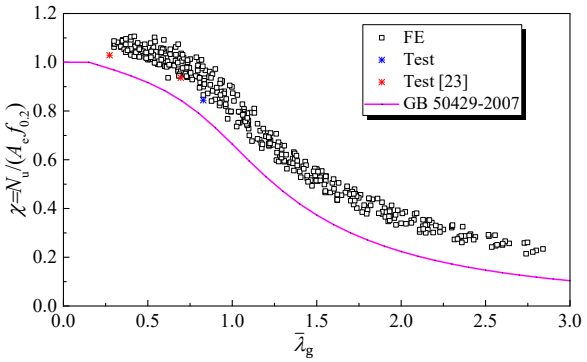

Fig. 13. Comparison of test/FE data with GB 50429-2007 for columns to local-flexural buckling

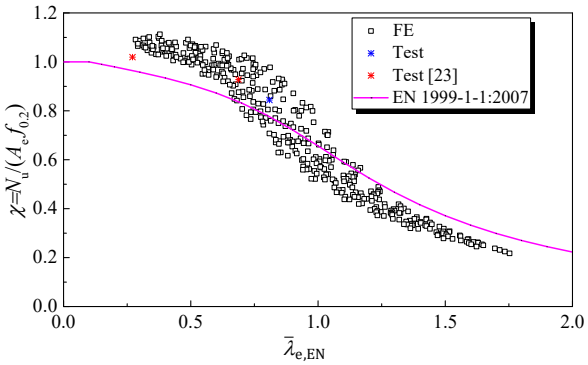

Fig. 14. Comparison of test/FE data with EN 1999-1-1:2007 for columns to local-flexural buckling

Table 8. Comparison of test/FE results with predicted strengths for columns to local-flexural buckling

Ratio	$N_{u,exp/FE}$ /$N_{u,GB}$	$N_{u,exp/FE}$ /$N_{u,EN}$	$N_{u,exp/FE}$ /$N_{u,AA}$	$N_{u,exp/FE}$ /$N_{u,AA-DSM}$	$N_{u,exp/FE}$ /$N_{u,AS/NZS}$	$N_{u,exp/FE}$ /$N_{u,GB,MLF1}$	$N_{u,exp/FE}$ /$N_{u,GB,MLF2}$	$N_{u,exp/FE}$ /$N_{u,DSM-GB}$
Mean	1.353	0.994	0.998	0.955	0.969	1.056	1.056	1.056
COV	0.170	0.152	0.117	0.119	0.124	0.094	0.087	0.058

In the framework of GB 50429-2007, three ways of modifications were proposed to improve the accuracy of axial compression resistance predictions of RHS columns to local-flexural buckling. The first one was to adopt $\alpha = 0.96$ and $\bar{\lambda}_0 = 0.63$ in the linear imperfection term $\eta = \alpha(\bar{\lambda}_g - \bar{\lambda}_0)$ and take $A_{e,GB}$ into account for determining χ_{GB}. The second proposal was to use the nonlinear imperfection term $\eta = \alpha[(\bar{\lambda}_{e,GB}+\mu)^{\xi} - \bar{\lambda}_0]$ due to the natural nonlinear relationship between η and $\bar{\lambda}_{e,GB}$, in which $\alpha = 0.16$, $\bar{\lambda}_0 = \mu = 0.28$ and $\xi = 3.0$. Note that $A_{e,GB}$ shall be used to obtain χ_{GB}. The third one was related to the DSM, which has been extensively employed to obtain the axial compression resistances of thin-walled members associated with element local buckling and member overall buckling, as proposed by Eqs. (7) - (10)

$$N_{ce} = \frac{f_{0.2} A_g}{\phi + \sqrt{\phi^2 - \bar{\lambda}_g^2}} \tag{7}$$

$$N_{cl} = \begin{cases} N_{ce} & \text{for } \bar{\lambda}_{l,DSM} \le 0.796 \\ \left(\dfrac{1.33}{\bar{\lambda}_{l,DSM}^{0.9}} - \dfrac{0.42}{\bar{\lambda}_{l,DSM}^{1.8}} \right) N_{ce} & \text{for } \bar{\lambda}_{l,DSM} > 0.796 \end{cases} \tag{8}$$

$$\phi = 0.5\{1+0.16[(\bar{\lambda}_g+0.28)^3-0.28]+\bar{\lambda}_g^2\} \tag{9}$$

$$\bar{\lambda}_{l,DSM} = \sqrt{N_{ce} / (\sigma_{cr} A_g)} \tag{10}$$

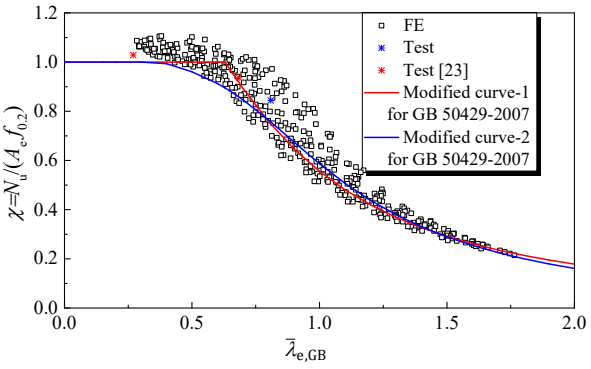

Fig. 15. Comparison of test/FE data with modified GB 50429-2007 for columns to local-flexural buckling

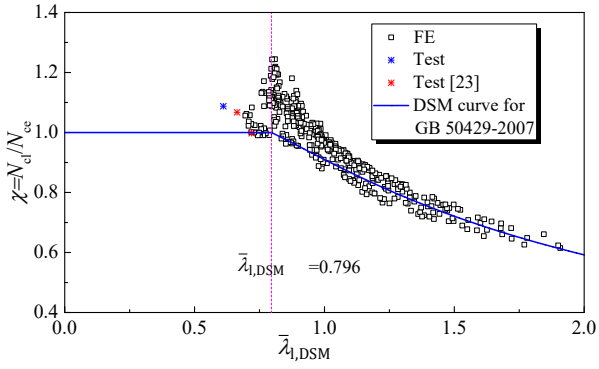

Fig. 16. Comparison of test/FE data with modified DSM for columns to local-flexural buckling

It should be noted that the flexural buckling resistances (N_{ce}) and corresponding buckling resistances allowing for local buckling (N_{cl}) shall be computed on the basis of the gross sectional area (A_g).

Accordingly, the three modified local-flexural buckling curves are displayed in Figs. 15 and 16. As can be seen from Table 8 that the mean ratios of test/FE data to calculated results by three modified design methods based on GB 50429-2007 were all 1.056 with COVs of 0.094, 0.087 and 0.058, respectively, which were much more accurate and stable compared to those from codified GB 50429-2007, especially for the modified DSM based on GB 50429-2007.

5. Reliability analyses

The reliability analyses were performed to evaluate the safety levels of current codified rules in Chinese code (GB 50429-2007), European standard (EN 1999-1-1:2007), American specification (AA-2015) and Australian/New Zealand standard (AS/NZS 1664.1:1997), as well as relevant modified methods for 7A04-T6 high-strength aluminium alloy RHS columns undergoing flexural buckling or local-flexural buckling. Note that the partial safety factors corresponding to various specifications were stated in Section 4.1-4.4, and they were used to derive reliability indices.

5.1 Resistance and load variables

The key statistical parameters, including the material strength, geometric dimensions and the model error, were determined according to the work in this paper and available data on high-strength aluminium alloy coupon and member tests [21-26]. The mean value of $f_{0.2}$ and COV were obtained as 539 MPa and 0.047 respectively. The geometric dimensions are taken as the nominal width, height and thickness of a cross-section divided by their measured ones, and the mean value and COV were determined as 1.004 and 0.015, respectively. The model error is defined as the ratio of the test/FE results to predicted axial compression resistances, and mean values and COVs are listed in Tables 7 and 8. Note that the three random variables about the column resistance were all assumed to be normally distributed.

The dead load (S_{DL}), residential live load (S_{RLL}), office live load (S_{OLL}) and wind load (S_{WL}) were considered to construct three types of load combinations, as shown in Table 9. The statistical parameters

of the four loads (i.e. S_{DL}, S_{RLL}, S_{OLL} and S_{WL}) in terms of the distribution type, ratio of nominal to mean values and COVs are specified in References [2, 35, 36], corresponding to aforementioned four standards. The load ratios of $\rho = S_{RLL}/S_{DL}$, S_{OLL}/S_{DL}, S_{WL}/S_{DL} were further introduced to assess the influence of the load ratio on reliability indices, and various values of ρ = 0.1, 0.25, 0.5, 1.0, 2.0, 3.0 and 4.0 were considered in this paper.

Table 9. Load combinations of different design standards

Combination	GB 50068-2018 [37]	EN1990 [38]	ASCE7-2010 [39]
S_{DL}+S_{RLL}	1.3S_{DL}+1.5S_{RLL}	1.35S_{DL}+1.5S_{RLL}	1.2S_{DL}+1.6S_{RLL}
S_{DL}+S_{OLL}	1.3S_{DL}+1.5S_{OLL}	1.35S_{DL}+1.5S_{OLL}	1.2S_{DL}+1.6S_{OLL}
S_{DL}+S_{WL}	1.3S_{DL}+1.5S_{WL}	1.35S_{DL}+1.5S_{WL}	0.9S_{DL}+1.0S_{WL}
Application object	GB 50429-2007	EN 1999-1-1:2007	AA-2015, AS/NZS 1664.1:1997

Since the partial safety factor and design strength of the 7A04-T6 high-strength aluminium alloy are not reported in current standards, the partial safety factors mentioned in Section 4.1-4.4 for 6xxx series aluminium alloys were employed herein. Based on the 50 collected tensile coupon results [21-26], the statistical design yield strength was taken as 410 MPa and 445 MPa for GB 50429-2007 and EN 1999-1-1:2007, respectively, and the nominal yield strength was obtained as 490 MPa for AA-2015 and AS/NZS 1664.1:1997. The statistical parameters of the loads, load combinations and partial safety factor for the DSM are the same as those of GB 50429-2007 in view of the manufacture and application of 7A04-T6 high-strength aluminium alloy RHS columns in China.

5.2 Reliability analysis results

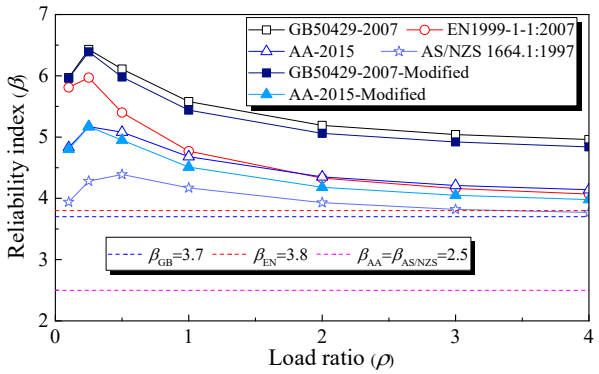

Fig. 17. Reliability indices of the design methods for columns to flexural buckling

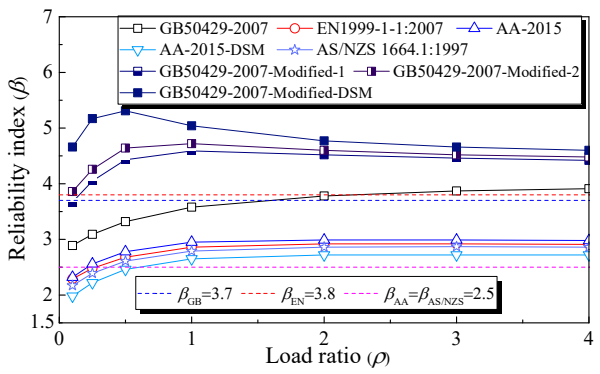

Fig. 18. Reliability indices of the design methods for columns to local-flexural buckling

The reliability analysis results of RHS columns to flexural buckling and local-flexural buckling of the current codified and relevant modified design methods are illustrated in Figs. 17 and 18, respectively, in which β is the mean indices for all the three load combinations under the same ρ. The target values specified in the four standards, including $\beta_{GB} = 3.7$, $\beta_{EN} = 3.8$, $\beta_{AA} = \beta_{AS/NZS} = 2.5$, are also displayed in figures. As illustrated in Fig. 16, the mean values of β for GB 50429-2007, EN 1999-1-1:2007, AA-2015 and AS/NZS 1664.1:1997 and modifications on GB 50429-2007 and AA-2015 were 5.61, 4.93, 4.64, 4.04, 5.51, and 4.52, respectively, which were all greater than the corresponding target index, indicating these design rules for RHS columns undergoing flexural buckling were reliable. While for the RHS columns undergoing local-flexural buckling, GB 50429-2007, EN 1999-1-1:2007, the DSM in AA-2015 and AS/NZS 1664.1:1997 failed to achieve respective target index, with mean values of β being 3.49, 2.72, 2.50 and 2.65, respectively. The β obtained from the three ways of modifications on GB 50429-2007 were all in excess of the target value of 3.7, which significantly increased by 23%, 27% and 40%, respectively, when compared with GB 50429-2007 results, demonstrating that all the three ways of modifications on GB 50429-2007 were reliable and safe to predict the axial compression resistances of high-strength aluminium alloy RHS columns to local-flexural buckling.

6. Conclusions

The buckling performance of 7A04-T6 high-strength aluminium alloy RHS columns under axial compression was studied by test and FE analyses. The test programme consisted of material property tests, initial geometric imperfection measurements and column tests. Additional resistance results, including 900 FE data for columns to flexural buckling and 396 FE data for columns to local-flexural buckling, were generated by verified FE models. The test and FE results of 7A04-T6 high-strength aluminium alloy RHS columns were adopted to compare against current codified design methods specified in Chinese, European, American and Australian/New Zealand standards. It was found that the

former three design approaches provided conservative resistance predictions by about 9%, with reliability indices being all greater than their corresponding target values, while slightly unsafe results were found for AS/NZS 1664.1:1997 for RHS columns to flexural buckling. With regard to RHS columns to local-flexural buckling, the predictions of GB 50429-2007 were the most conservative by approximately 35%, while conservative results under smaller member slenderness and overestimated ones under larger member slenderness were observed for EN 1999-1-1:2007, AA-2015 and AS/NZS 1664.1:1997, leading to a great dispersion of data and failing to reach expected reliability indices.

On the basis of the evaluation results of current codified design approaches, new design curves for 7A04-T6 high-strength aluminium alloy RHS columns to flexural buckling were separately proposed for GB 50429-2007 and AA-2015, with higher accuracy and reliability level. Additionally, three ways of proposals to the linear imperfection term, nonlinear imperfection term and the DSM combined with nonlinear imperfection term were separately suggested based on GB 50429-2007 for 7A04-T6 high-strength aluminium alloy RHS columns to local-flexural buckling, offering safe and accurate predictions according to the mean ratios and COVs of test/FE-to-predictions as well as reliability analyses.

Acknowledgements

The financial supports from the National Natural Science Foundation of China (Grants NO. 52108154 and No.51878377), the China National Postdoctoral Program for Innovative Talents (Grant No. BX20200193) and the China Postdoctoral Science Foundation (Grant No. 2021M691826) are well acknowledged.

References

[1] Georgantzia E, Gkantou M, Kamaris G. Aluminium alloys as structural material: A review of research. Engineering Structures, 2021, 227: 111372.

[2] GB 50429-2007. Code for design of aluminium structures. Beijing: China Planning Press, 2007. (in Chinese)

[3] EN 1999-1-1:2007. Eurocode 9: Design of aluminium structures. Part 1-1: General structural rules-General

structural rules and rules for buildings. European Committee for Standarization Brussels, 2007.

[4] AA-2015. Aluminum design manual. The Aluminum Association, Washington DC, 2015.

[5] AS/NZS 1664.1:1997. Aluminum Structures Part 1: Limit State Design. Australian/New Zealand Standard, Standard Australia, Sydney, Australia, 1997.

[6] Wang ZX, Wang YQ, Sojeong J, Ouyang YW. Experimental investigation and parametric analysis on overall buckling behavior of large-section aluminum alloy columns under axial compression. Thin-Walled Structures, 2018, 122: 585-596.

[7] Zhang Y, Wang YQ, Li BB, Wang ZX, Liu XC, Zhang JG, Ouyang YW. Structural behaviour of the aluminium alloy Temcor joints and Box-I section hybrid gusset joints under combined bending and shear. Engineering Structures, 2021, 249: 113380.

[8] Zhu JH, Young B. Tests and design of aluminum alloy compression members. Journal of Structural Engineering, 2006, 132(7): 1096-1107.

[9] Zhu JH, Young B. Aluminum alloy tubular columns-Part II: Parametric study and design using direct strength method. Thin-Walled Structures, 2006, 44: 969-985.

[10] Zhu JH, Young B. Experimental investigation of aluminum alloy circular hollow section columns. Engineering Structures, 2006, 28: 207-215.

[11] Zhu JH, Li ZQ, Su MN, Young B. Behaviour of aluminium alloy plain and lipped channel columns. Thin-Walled Structures, 2019, 135: 306-316.

[12] Su MN, Young B, Gardner L. Testing and design of aluminium alloy cross-sections in compression. Journal of Structural Engineering, 2014, 140(9): 04014047.

[13] Adeoti GO, Fan F, Wang YJ, Zhai XM. Stability of 6082-T6 aluminium alloy columns with H-section and rectangular hollow sections. Thin-Walled Structures, 2015, 89: 1-16.

[14] Wang YQ, Yuan HX, Chang T, Du XX, Yu M. Compressive buckling strength of extruded aluminium alloy I-section columns with fixed-pinned end conditions. Thin-Walled Structures, 2017, 119: 396-403.

[15] Feng R, Young B. Experimental investigation of aluminum alloy stub columns with circular openings. Journal of Structural Engineering, 2015, 141(11): 04015031.

[16] Feng R, Liu JR. Numerical investigation and design of perforated aluminium alloy SHS and RHS columns. Engineering Structures, 2019, 199: 109591.

[17] Roy K, Chen BS, Fang ZY, Uzzaman A, Chen X, Lim JBP. Local and distortional buckling behaviour of back-to-back built-up aluminium alloy channel section columns. Thin-Walled Structures, 2021, 163: 107713.

[18] Fang ZY, Roy K, Chen BS, Xie ZX, Lim JBP. Local and distortional buckling behaviour of aluminium alloy back-to-back channels with web holes under axial compression. Journal of Building Engineering, 2022, 47: 103837.

[19] Wang YQ, Wang ZX. Experimental investigation and FE analysis on constitutive relationship of high strength aluminum alloy under cyclic loading. Advances in Materials Science and Engineering, 2016: 1-16.

[20] Yun X, Wang ZX, Gardner L. Full-range stress-strain curves for aluminium alloys. Journal of Structural Engineering, 2021, 147(6): 04021060.

[21] Wang ZX, Wang YQ, Yun X, Gardner L, Hu XG. Experimental and numerical study of fixed-ended high-strength aluminum alloy angle-section columns. Journal of Structural Engineering, 2020, 146(10): 04020206.

[22] Wang YQ, Wang ZX, Hu XG, Han JK, Xing HJ. Experimental study and parametric analysis on the stability behaviour of 7A04 high-strength aluminum alloy angle columns under axial compression. Thin-Walled Structures, 2016, 108: 305-320.

[23] Rong B, Guo Y, Li ZY. Study on the stability behavior of 7A04-T6 aluminum alloy square and rectangular hollow section columns under axial compression. Journal of Building Engineering, 2022, 45: 103652.

[24] Yuan Lin, Zhang QL, Ouyang YW. Experimental investigation and design method of the flexural bucklingresistance of high-strength aluminum alloy H-columns. Structures, article in press.

[25] Hu YW, Rong B, Zhang RY, Zhang YC, Zhang S. Study of buckling behaviour for 7A04-T6 aluminum alloy rectangular hollow columns. Thin-Walled Structures, 2021, 169: 108410.

[26] Rong B, Zhang YC, Zhang S, Li ZY. Experiment and numerical investigation on the buckling behavior of 7A04-T6 aluminum alloy columns under eccentric load. Journal of Building Engineering, 2022, 45: 103625.

[27] GB/T 228.1-2010. Metallic materials-Tensile testing-Part 1: Method of test at room temperature. Beijing: China Standards Press, 2008. (in Chinese)

[28] Zhang Y, Wang YQ, Wang ZX, Bu YD, Fan SG, Zheng BF. Experimental investigation and numerical analysis of pin-ended extruded aluminium alloy unequal angle columns. Engineering Structures, 2020, 215: 110694.

[29] Buchanan C, Real E, Gardner L. Testing, simulation and design of cold-formed stainless steel CHS columns. Thin-Walled Structures, 2018, 130: 297-312.

[30] Dassault Systemes. ABAQUS/Standard user's manual volumes I-III and ABAQUS CAE manual - Version 6.19. UK: Simulia Corporation; 2014.

[31] Yuan HX, Wang YQ, Chang T, Du XX, Bu YD, Shi YJ. Local buckling and postbuckling strength of extruded aluminium alloy stub columns with slender I-sections. Thin-Walled Structures, 2015, 90: 140-149.

[32] Zhi XH, Wang YQ, Li BB, Zhang Y, Fan SG, Ouyang YW. Experimental study on local buckling behavior of 7075-T6 high-strength aluminum alloy stub columns under axial compression. Journal of Tianjin University (Science and Technology), Accept. (in Chinese)

[33] Gardner L, Nethercot DA. Numerical modeling of stainless steel structural components-A consistent approach. Journal of Structural Engineering, 2004, 130(10): 1586-1601.

[34] Li Z, Schafer BW. Buckling analysis of cold-formed steel members with general boundary conditions using CUFSM: conventional and constrained finite strip methods, Missouri University of Science and Technology, Rolla, MO, USA, 2010.

[35] SAKO. Joint Committee of NKB and INSTA-B. Design basis of structures. Proposal for modification of partial safety factors in Eurocodes. 1999.

[36] Maria MS, Andrzej SN. Calibration of design code for buildings (ACI 318): Part 2-Reliability analysis and resistance factors. ACI Structural Journal, 2003, 100: 383-391.

[37] GB 50068-2018. Unified standard for reliability design of building structures. Beijing: China Construction Industry Press, 2018 (in Chinese).

[38] Eurocode. Basis of structural design. BS EN 1990: 2002, European Committee for Standardization (CEN), 2002.

[39] ASCE 7-10. Minimum design load for buildings and other structures. American Society of Civil Engineers, Reston, 2010.